Fluid Dynamics in a Bubble Column: New Experiments and Simulations

Rzehak, R.; Krauß, M.; Kováts, P.; Zähringer, K.;

Originally published:

November 2016

International Journal of Multiphase Flow 89(2017), 299-312

DOI: https://doi.org/10.1016/j.ijmultiphaseflow.2016.09.024

Perma-Link to Publication Repository of HZDR:

https://www.hzdr.de/publications/Publ-23757

Fluid Dynamics in a Bubble Column: New Experiments and Simulations

Roland Rzehak[1*], Manuel Krauß[1], Péter Kováts[2], Katharina Zähringer[2]

[1] Helmholtz-Zentrum Dresden – Rossendorf, Institute of Fluid Dynamics,
Bautzner Landstrasse 400, D-01328 Dresden, Germany
[2] Laboratory of Fluid Dynamics and Technical Flows, Otto-von-Guericke-Universität
Magdeburg. Universitätsplatz 2, D-39106 Magdeburg, Germany

Abstract

Bubble columns are a common type of multiphase reactors used in many chemical engineering applications. Optimization and scale-up of bubble column processes is a complex task that can greatly benefit from multiphase CFD simulations. Calculations on industrial scales become feasible by the Euler-Euler two-fluid model, but suitable closure relations describing interfacial exchange processes are needed for practical application. Concerning pure fluid dynamics of dispersed gas-liquid multiphase flow an ongoing effort has led to a validated set of closures that is applicable under a rather broad range of conditions. The availability of new experimental data with large spatial and temporal resolution and high accuracy for a comprehensive set of observables and a range of different conditions provides the opportunity for further testing of this model. In this way the reliability of the obtained predictions is continually increased.

Keywords: bubble-columns, CFD simulation, Euler Euler two fluid model, shadowgraphy, PIV, model validation

[*] Corresponding author email: r.rzehak@hzdr.de

1 INTRODUCTION

Bubble columns (Shah et al. 1982, Deckwer 1992, Kantarci et al. 2005) are frequently used as multiphase reactors since they offer simple construction without any moving parts. At the same time a relatively large interfacial area leads to good heat- and mass-transfer properties. On the downside there is significant backmixing, which may adversely affect product conversion. Despite its simple construction, the flow inside a bubble column is quite complex and a detailed understanding is still lacking to date.

Typical for bubbly flows is the existence of widely disparate length scales, most prominently the size of the individual bubbles at the small end and the dimension of the domain occupied by the fluid at the large end. A computational treatment becomes feasible within the Eulerian two-fluid framework of interpenetrating continua in which the small scales are eliminated by an averaging procedure and only the large scales are resolved. However, to obtain a closed system of equations, the physics on the scale of individual bubbles or groups thereof has to be modelled by so-called closure relations.

A large number of works exists, in each of which largely a different set of closure relations is compared to a different set of experimental data. Systems that are of considerable practical interest, and have therefore been considered particularly extensively, are bubble columns (Marschall et al. 2010, Jakobsen et al. 2005, Sokolichin et al. 2004), airlift columns (Luo and Al-Dahan 2011, Talvy et al. 2007) and bubbly pipe flows (Podowski 2009, Serizawa and Tomiyama 2003). The relevance of various forces acting on the bubbles and suitable correlations describing their strength, depending on the local flow parameters, have been assessed (Masood and Delgado 2014, Silva et al. 2012, Diaz et al. 2009, Hibiki and Ishii 2007). Different general frameworks for the description of turbulence have been compared (Masood and Delgado 2014, Silva et al. 2012, Selma et al. 2010a, Ekambara and Dhotre 2010, Tabib et al. 2008, Zhang et al. 2006) and a number of possibilities to include the bubble induced contribution to the turbulence have been considered (Colombo and Fairweather 2015, Selma et al. 2010a, Laborde-Boutet et al. 2009, Politano et al. 2003, Troshko and Hassan 2001, Morel 1997). Finally, several available frameworks to include processes of bubble coalescence and breakup have been applied (Buffo, A., Marchisio 2014, Selma et al. 2010b, Fox 2007, Sanyal et al. 2005) and specific expressions for the rates of these processes have been employed (Chen et al. 2005, Wang et al. 2005).

For the limited range of conditions to which each model variant is applied, reasonable agreement with the data is mostly obtained, but due to a lack of comparability between the individual works, no complete, reliable, and robust formulation has been achieved so far. Moreover, the models usually contain a number of empirical parameters that have been adjusted to match the particular data, that were used in the comparison. Predictive simulation, however, requires a model that works without any adjustments within the targeted domain of applicability.

As a step towards this goal, an attempt has been made to collect the best available description for all aspects known to be relevant for adiabatic bubbly flows where only momentum is exchanged between liquid and gas phases (Rzehak et al. 2012, Rzehak and Krepper 2013a,b, Rzehak and Kriebitzsch 2015). Apart from interest in its own right, results obtained for this restricted problem also provide a good starting point for the investigation of more complex situations, including heat and mass transport and possibly phase change or chemical reactions.

This baseline model has since been validated for a number of different test cases including bubbly flow in pipes (Rzehak et al. 2014, Rzehak and Krepper 2015, Rzehak et al. 2015, Rzehak et al. 2016), bubble columns (Rzehak et al. 2014, Ziegenhein et al. 2015, Ziegenhein et al 2016, Rzehak et al. 2016), and airlift-columns (Liao et al. 2016, Rzehak et al. 2016). The

applicability of a single model to such diverse configurations makes it a well-suited starting point for further investigations, aiming at an expansion of the range of applicability, as well as an improvement of the achieved accuracy. These activities are part of a continuously ongoing development effort.

In the present work, the baseline model is applied to a further bubble column test case where the sparger consists of four nozzles arranged in a line (Kovats et al. 2015, 2016). This permits taking data in a full plane spanned by the column axis and a column diameter. The latter can be chosen along the line formed by the needles or perpendicular to it. The occurrence of bubbles, their diameters, trajectories and velocities have been recorded by shadowgraphy and the liquid velocity, including turbulence quantities, has been measured by High-Speed-PIV. Comparison of the two-dimensional numerical and experimental fields provides a unique opportunity for validation of the baseline model beyond the previous numerical investigations.

2 DESCRIPTION OF EXPERIMENTS

A full description of the experimental set-up has been published before (Kovats et.al. 2016). Therefore only the main information concerning the bubble column geometry, process parameters and measurement techniques is given here.
The bubble column has an inner diameter of 0.142 m (Fig.1, left) and is made from acrylic glass. In the bottom, 4 stainless steel nozzles with an inner diameter of 0.25 mm are placed for the production of gas bubbles with a diameter of 2.5-3.5 mm. The needles are arranged in a line, spaced by 22 mm, and extend by 13 mm into the column. The column is filled with 11.5 l de-ionised water, which results in a fill height of 0.73 m, when no gas is present. Pressurized air and CO_2-gas from a bottle have been used to form the bubbles.

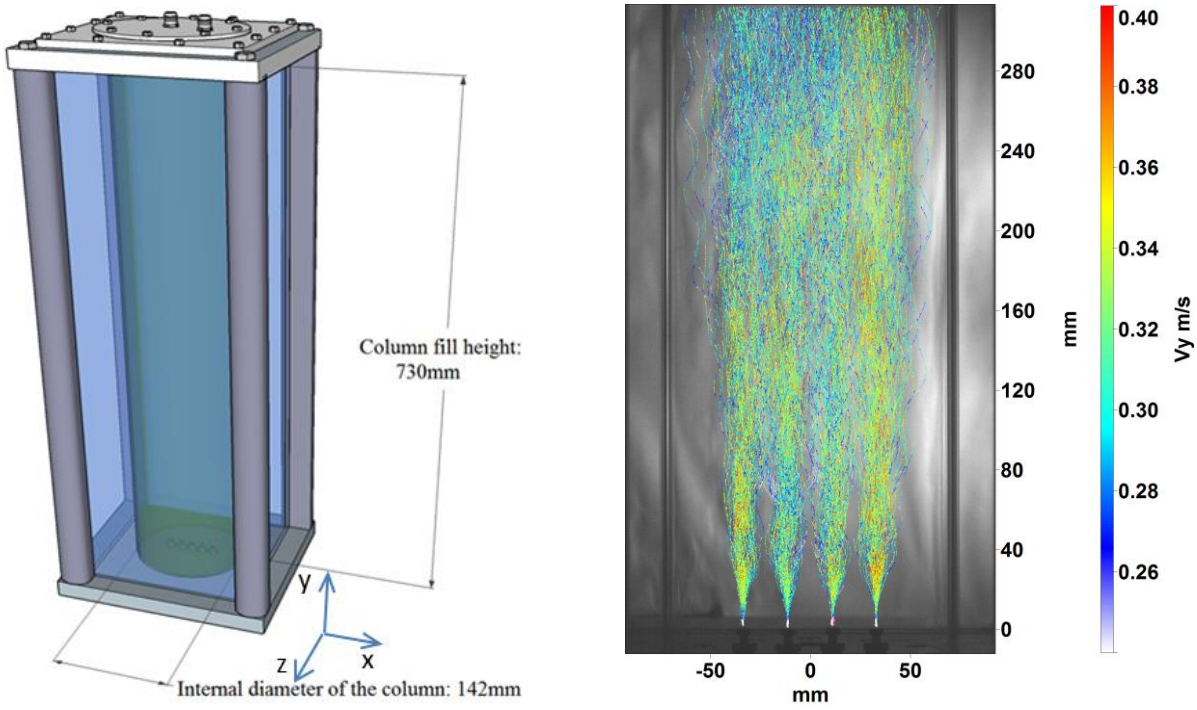

Figure 1: Bubble column geometry (left) and example of bubble trajectories, coloured with the local vertical velocity (right).

2.1 Bubble identification, bubble location, velocity and diameter

To investigate the gas phase, the shadowgraphy technique has been used to determine bubble location, velocity and diameter. For these measurements, an Imager pro HS 4M CCD camera has been used with a resolution of 2016 x 2016 pixels. The images were taken with a frame rate of 0.1 kHz in the lower 0.3 m of the bubble column. Two Dedocool halogen lights reflected by a white background were used as illumination source. Four series of 250 images were taken for each parameter to obtain sufficient statistics. The images have been treated with Davis-Software from LaVision and first of all a previously recorded background-image was removed. Then bubble location, velocity, diameter and geometrical parameters have been determined (Fig. 1 right). The direction of view was perpendicular to the line formed by the 4 needles (front view) and in some cases also along this line (side view). The acquired experimental results are summarized in Table 1.

Table 1. Measurement results showing mean bubble diameters (mm) and mean bubble vertical velocities (m/s) for the different gas flow rates (l/h) used.

Gas flow rate (l/h)	Average bubble diameter (mm)	Average bubble vertical velocity (m/s)
3.5	2.3	0.33
5	2.5	0.33
7.5	2.9	0.31
10	3.1	0.31

A previous parameter study (Kovats et al. 2015) showed, that only the gas flow rate has a noticeable influence on the velocity and size of the bubbles in this region. The higher the flow rate, the larger is the bubble diameter and the broader is the bubble size distribution (Fig. 2). In this bubble size range, bubbles follow a three-dimensional helical or zig-zag path. Therefore their velocities are decreasing as shown in Figure 3.

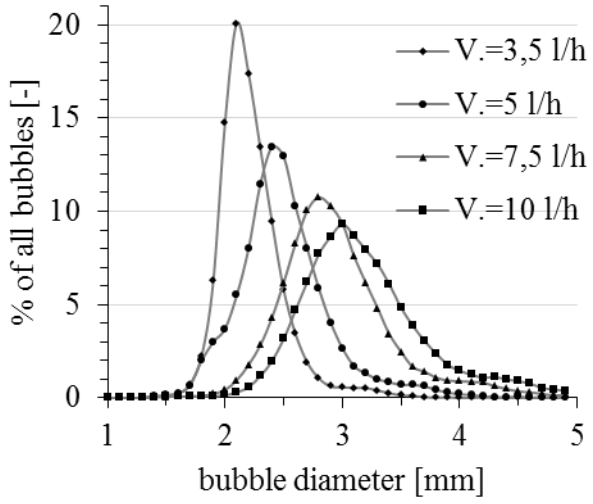

Figure 2. Bubble size distribution as function of gas flow rate.

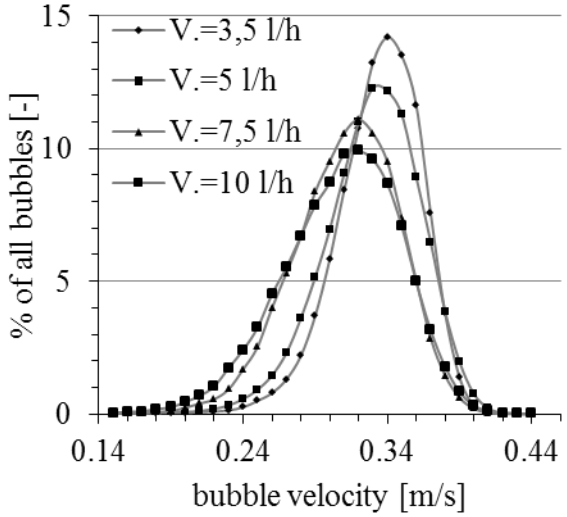

Figure 3. Bubble velocity distribution as function of gas flow rate.

2.2 Calculation of gas fractions

To facilitate comparison with the Euler-Euler simulation results, the measured bubble locations and sizes have to be converted into a gas fraction field giving the probability to find a bubble at a certain position. To this end, the measurement plane has been covered with a grid of 5.0 mm spacing in the vertical and 2.5 mm in the lateral direction. This value was determined from several trials as a good compromise between resolution and smoothness of the resulting gas fraction field and is of a size comparable to the computational grid used in the simulations. Then for each grid cell, the number count of bubble centers falling inside this cell was accumulated. All 4 x 250 images were used in this process. The resulting number count N_B was multiplied by the average bubble volume V_B and divided by the cell volume V_C, i.e.

$$\alpha_G = N_B \frac{V_B}{V_C} \quad . \tag{1}$$

For the cell volume it has to be considered that each grid cell has a depth corresponding to the depth of field of the camera system, which was 40 mm. For the final comparison, the simulated gas fractions also have to be averaged within a range of this size centered around the observation plane.

2.3 Liquid phase flow

To examine the hydrodynamics of the water phase in the bubble column, high-speed PIV measurements have been carried out. For the measurements, an Imager pro HS 4M CCD camera has been used with a resolution of 2016 x 2016 pixels. The camera was equipped with a Nikon AF Micro Nikkor 60mm f/2.8D lens. As tracer particles, polymethyl methacrylate (PMMA) Rhodamin B particles have been used with a mean diameter of 10 µm. To get continuous time-resolved PIV results, the images have been acquired with a frame rate of 1 kHz as time series. The bubble column has been divided into five measurement sections (Fig.4, left, S1-S5) with a 10 mm overlap. To illuminate the particles, a high speed Nd:YLF laser (Litron) with a wavelength of 527 nm and an energy of 4.45 mJ/P has been used. The laser beam has been expanded by a light sheet optics to a 159 x 159 mm^2 region of interest.
In each measurement section 20 image sets have been acquired, where each set contains (due to memory limitation) 3140 images, acquired during 3.14 s. This means that 62800 images are taken at each position, covering a time of about 1 minute, for further evaluation of mean velocities and turbulence quantities.

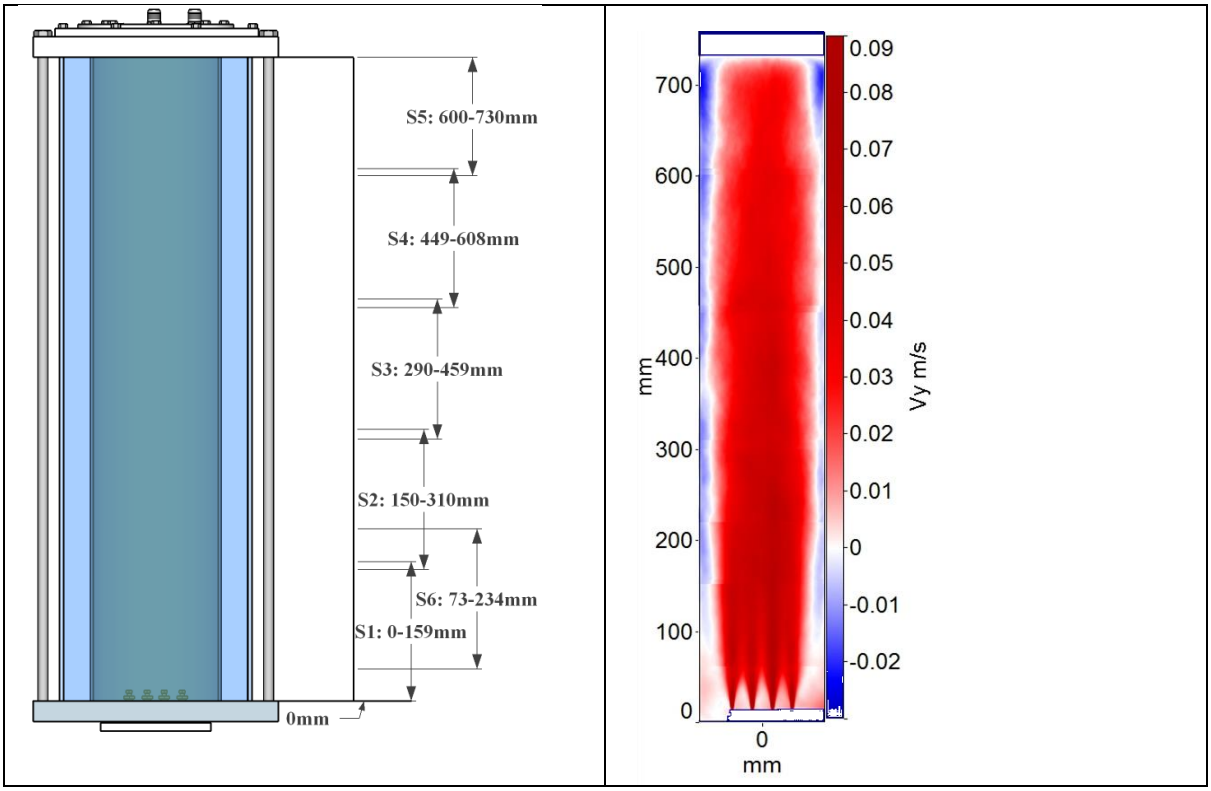

Figure 4: Measurement sections for HS-PIV experiment (left). Average vertical liquid velocity in overlapped result with six sections (right).

For acquisition and postprocessing of the raw images, DaVis 8.3 (LaVision) has been used. For the vector calculation a single-pass cross-correlation PIV algorithm has been used, with an interrogation window size of 16 x 16 pixels. To remove false vectors and refine the vector field, especially in the vicinity and shadows of the bubbles, vector postprocessing has been applied after the first processing step. An allowable vector range filter has been first employed according to the former experiments (Kováts et.al. 2016). Then with the help of a median filter the vectors have been refined. For this, the median vector from the 8 neighbouring interrogation areas is computed and then compared to the vector in the center. Its deviation from the neighbouring vectors, is evaluated and the highest (but in some cases wrong) correlation peak was replaced by the second, third or fourth highest correlation peak, until a sufficient agreement is obtained within the neighbourhood. The current vector position was disabled if none of the four peaks were in the allowed range of the median vector. These few disabled areas were afterwards replaced with an interpolated value from the 8 neighbours.

For the average velocity fields all 62800 images have been averaged at each section. The averaged images show an almost symmetric velocity field in each section (e.g. in Fig. 4 right, the vertical velocity component). As expected, a large ascending part in the centre of the column and a thin descending zone near the wall can be recognized. When overlapping the different measured fields, slight deviations of the velocity values become visible. Especially in a height of 150 mm the deviation was rather strong. Therefore a sixth measurement position has been introduced to decrease these deviations (Fig. 4, left S6). Due to memory considerations (2500 Gbytes for raw images, plus 1500 Gbytes for the treated images), a further increase of the number of images at each measurement position was unfortunately not possible for the moment.

3 BASELINE MODEL FOR SIMULATION OF BUBBLY FLOWS

The conservation equations of the Euler-Euler two-fluid model have been discussed at length in a number of books (e.g. Drew and Passman 1998, Yeoh and Tu 2010, Ishii and Hibiki 2011) and a broad consensus has been reached, so this general framework will not be repeated here. Closure relations required to complete the model, in contrast, are still subject to considerable variation between researchers. Here, a baseline model is adopted that has emerged from a series of previous studies (Rzehak and Krepper 2013a, Rzehak et al. 2014, Ziegenhein et al. 2015, Rzehak and Krepper 2015, Rzehak et al. 2015, Ziegenhein et al 2016, Liao et al. 2016, Rzehak et al. 2016). Details of the model are given in section 3.1 for the bubble forces and in section 3.2 for bubble-induced turbulence. Other aspects of the models are specified in section 3.3, namely bubble size, boundary conditions and geometry.

3.1 Bubble Forces

Concerning momentum exchange between liquid and gas phase, drag, lift, wall, and turbulent dispersion forces are considered in the baseline model. The correlations are expressed in terms of dimensionless numbers, namely the Reynolds number $Re = |\mathbf{u}_G - \mathbf{u}_L| \; d_B \; \nu_L^{-1}$, the Eötvös number $Eo = (\rho_L - \rho_G) \; g \; d_B^{\,2} \; \sigma^{-1}$, and the Morton number $Mo = (\rho_L - \rho_G) \; \rho_L^{-2} \; g \; \nu_L^{\,4} \; \sigma^{-3}$.

3.1.1 Drag Force

The drag force reflects the resistance opposing bubble motion relative to the surrounding liquid. The corresponding gas-phase momentum source is given by

$$\mathbf{F}^{drag} = -\frac{3}{4 d_B} C_D \rho_L \alpha_G \left|\mathbf{u}_G - \mathbf{u}_L\right| \; (\mathbf{u}_G - \mathbf{u}_L) \; . \tag{2}$$

The drag coefficient C_D depends strongly on the Reynolds number *Re* and for deformable bubbles also on the Eötvös number *Eo*, but turns out to be independent of the Morton number *Mo*. A correlation distinguishing different shape regimes has been suggested by Ishii and Zuber (1979), namely

$$C_D = \max\left(C_{D,sphere}, \min\left(C_{D,ellipse}, C_{D,cap}\right)\right) , \tag{3}$$

where

$$\begin{aligned} C_{D,sphere} &= \frac{24}{\mathrm{Re}}\left(1 + 0.1 \; \mathrm{Re}^{0.75}\right) \\ C_{D,ellipse} &= \frac{2}{3}\sqrt{\mathrm{Eo}} \\ C_{D,cap} &= \frac{8}{3} \end{aligned} \quad . \tag{4}$$

This correlation was compared with an extensive data set on the terminal velocity of bubbles rising in quiescent liquids, covering several orders of magnitude for each of *Re*, *Eo* and *Mo* in (Tomiyama et al. 1998) with good agreement except at high values of *Eo*.

3.1.2 Lift Force

A bubble moving in an unbounded shear flow experiences a force perpendicular to the direction of its motion. The momentum source corresponding to this shear lift force, often simply referred to as lift force, can be calculated as (Zun 1980):

$$\mathbf{F}^{lift} = -C_L \rho_L \alpha_G (\mathbf{u}_G - \mathbf{u}_L) \times rot(\mathbf{u}_L) \ . \tag{5}$$

For a spherical bubble the shear lift coefficient C_L is positive so that the lift force acts in the direction of decreasing liquid velocity, i.e. in case of co-current pipe flow in the direction towards the pipe wall. Experimental (Tomiyama et al. 2002) and numerical (Schmidtke 2008) investigations showed, that the direction of the lift force changes its sign if a substantial deformation of the bubble occurs. From the observation of the trajectories of single air bubbles rising in simple shear flow of a glycerol water solution the following correlation for the lift coefficient was derived:

$$C_L = \begin{cases} \min[0.288 \tanh(0.121 \mathrm{Re}),\ f(Eo_\perp)] & Eo_\perp < 4 \\ f(Eo_\perp) & for \quad 4 < Eo_\perp < 10 \\ -0.27 & 10 < Eo_\perp \end{cases} . \tag{6}$$

$$\text{with} \quad f(Eo_\perp) = 0.00105 Eo_\perp^3 - 0.0159 Eo_\perp^2 - 0.0204 Eo_\perp + 0.474$$

This coefficient depends on the modified Eötvös number given by

$$Eo_\perp = \frac{g(\rho_L - \rho_G) d_\perp^2}{\sigma} \ , \tag{7}$$

where $d_\perp$ is the maximum horizontal dimension of the bubble. It is calculated using an empirical correlation for the aspect ratio by Wellek et al. (1966) with the following equation:

$$d_\perp = d_B \sqrt[3]{1 + 0.163 \ Eo^{0.757}} \ , \tag{8}$$

where *Eo* is the usual Eötvös number. An important feature of the model Eqs. (6) – (8) proposed by (Tomiyama et al. 2002) is that the lift coefficient changes its sign at a certain bubble size, which for air bubbles in water is $d_B \approx 6$ mm.

The experimental conditions on which Eq. (6) is based, were limited to the range $-5.5 \le log_{10} Mo \le -2.8$, $1.39 \le Eo \le 5.74$ and values of the Reynolds number based on bubble diameter and shear rate $0 \le Re \le 10$. The water-air system at normal conditions has a Morton number $Mo = 2.63\text{e-}11$ which is quite different, but good results have nevertheless been reported for this case (Lucas and Tomiyama 2011).

3.1.3 Wall Force

A bubble translating next to a wall in an otherwise quiescent liquid also experiences a lift force. This wall lift force, often simply referred to as wall force, has the general form

$$\mathbf{F}^{wall} = \frac{2}{d_B} C_W \rho_L \alpha_G \left|\mathbf{u}_G - \mathbf{u}_L\right|^2 \hat{\mathbf{y}} \ , \tag{9}$$

where $\hat{\mathbf{y}}$ is the unit normal perpendicular to the wall pointing into the fluid. The dimensionless wall force coefficient C_W depends on the distance to the wall y and is expected to be positive so the bubble is driven away from the wall.
Based on the observation of single bubble trajectories in simple shear flow of a glycerol water solution Tomiyama et al. (1995) and later Hosokawa et al. (2002) concluded a functional dependence

$$C_W(y) = f(Eo)\left(\frac{d_B}{2y}\right)^2 \ . \tag{10}$$

In the limit of small Morton number the correlation

$$f(Eo) = 0.0217 \ \ Eo \tag{11}$$

can be derived from the data of Hosokawa et al. (2002). The experimental conditions on which Eq. (11) is based are $2.2 \le Eo \le 22$ and $-6.0 \le log_{10} Mo \le -2.5$. This is quite different from the water-air system with $Mo = 2.63e^{-11}$, but a recent investigation (Rzehak et al. 2012) has nonetheless shown that good predictions are obtained also for air bubbles in water.

3.1.4 Turbulent Dispersion Force

The turbulent dispersion force describes the effect of the turbulent fluctuations of liquid velocity on the bubbles. Burns et al. (2004) derived an explicit expression by Favre averaging the drag force as:

$$\mathbf{F}^{disp} = -\frac{3}{4} C_D \frac{\alpha_G}{d_B} \left|\mathbf{u}_G - \mathbf{u}_L\right| \frac{\mu_L^{turb}}{\sigma_{TD}} \left(\frac{1}{\alpha_L} + \frac{1}{\alpha_G}\right) \text{grad}\, \alpha_G \ . \tag{12}$$

In the same work, the expression for the so-called Favre averaged drag (FAD) model has also been compared with other suggestions, which all agree at least in the limit of low void fraction.
In analogy to molecular diffusion, σ_{TD} is referred to as a Schmidt number. In principle it should be possible to obtain its value from single bubble experiments also for this force by evaluating the statistics of bubble trajectories in well characterized turbulent flows, but to our knowledge this has not been done yet. A value of $\sigma_{TD} = 0.9$ is typically used.

3.1.5 Virtual Mass Force

When a bubble is accelerated, a certain amount of liquid has to be set into motion as well. This may be expressed as a force acting on the bubble as

$$\mathbf{F}^{VM} = -C_{VM}\rho_L\alpha_G\left(\frac{D_G\mathbf{u}_G}{Dt} - \frac{D_L\mathbf{u}_L}{Dt}\right), \tag{13}$$

where D_G / Dt and D_L / Dt denote material derivatives with respect to the velocity of the indicated phase. For the virtual mass coefficient a value of C_{VM} = 0.5 has been derived for isolated spherical bubbles in inviscid and creeping flows by Auton et al. (1988) and Maxey and Riley (1983), respectively. Results of direct simulations of a single bubble by Magnaudet et al. (1995) suggest that this value also holds for intermediate values of *Re*.

3.2 Two-phase Turbulence

Due to the small density and small special scales of the dispersed gas it suffices to consider turbulence in the continuous liquid phase for bubbly flows. We adopt a two equation turbulence model for the liquid phase with additional source terms describing bubble induced turbulence. The formulation given is equally applicable to either k-ε, k-ω or SST model, but the latter (Menter 2009) will be used presently.
Concerning the source term describing bubble effects in the k-equation there is large agreement in the literature (e. g. Kataoka et al. 1992, Troshko and Hassan 2001). A plausible approximation is provided by the assumption that all energy lost by the bubble due to drag is converted to turbulent kinetic energy in the wake of the bubble. Hence, the k-source becomes

$$S_L^k = \mathbf{F}_L^{drag}\cdot\left(\mathbf{u}_G - \mathbf{u}_L\right). \tag{14}$$

For the ε-source a similar heuristic is used as for the single phase model, namely the k-source is divided by some time scale τ so that

$$S_L^\varepsilon = C_{\varepsilon B}\frac{S_L^k}{\tau}. \tag{15}$$

Further modeling then focuses on the time scale τ proceeding largely based on dimensional analysis. This follows the same line as the standard modeling of shear-induced turbulence in single phase flows (Wilcox 1998), where production terms in the ε-equation are obtained by multiplying corresponding terms in the k-equation by an appropriate time scale, which represents the life-time of a turbulent eddy before it breaks up into smaller structures. In single phase turbulence the relevant variables are obviously k and ε, from which only a single time scale $\tau = k_L/\varepsilon_L$ can be formed. For the bubble-induced turbulence in two-phase flows the situation is more complex. Obviously there are two length and two velocity scales in the problem, where one of each is related to the bubble and the other to the turbulent eddies. From these, a total of four different time scales can be formed. In the absence of theoretical arguments

to decide which of these is the most relevant one, a comparison of all four alternatives has shown the best performance for the choice $\tau = d_B / \sqrt{k_L}$ (Rzehak and Krepper 2013a) and this is followed herein. For the coefficient $C_{\varepsilon B}$ a value of 1.0 to was found to give reasonable results.
For use with the SST model, the ε-source is transformed to an equivalent ω-source which gives

$$S_L^{\omega} = \frac{1}{C_{\mu} k_L} S_L^{\varepsilon} - \frac{\omega_L}{k_L} S_L^{k} \ . \tag{16}$$

This ω-source is used independently of the blending function in the SST model since it should be effective throughout the fluid domain.
Since bubble-induced effects are included in k and ε / ω due to the respective source terms, the turbulent viscosity is evaluated from the standard formula

$$\mu_L^{\ turb} = C_{\mu} \rho_L \frac{{k_L}^2}{\varepsilon_L} \tag{17}$$

The effective viscosity is simply $\mu_L^{eff} = \mu_L^{mol} + \mu_L^{turb}$.
Boundary conditions on k and ε / ω are taken the same as for the single phase case, which is consistent with the view that the full wall shear stress is exerted by the liquid phase which contacts the full wall area. A single phase wall function is employed to avoid the need to resolve the viscous sublayer.
All turbulence model parameters take their usual single phase values for the presently investigated tests.

3.3 Other Model Aspects

Bubble size is a parameter appearing in all of the correlations described above and thus needs to be defined. Based on the experimental findings, a monodisperse approximation is applied, and the average of the measured distribution is used for the bubble size.
Also needed are values for the material properties. These are taken to be constant with values given in Table2.

Table 2: Material properties at atmospheric pressure and 25°C temperature.

	water (L)	air (G)	CO_2 (G)
ρ [kg m^{-3}]	997	1.185	1.840
μ [kg m^{-1} s^{-1}]	$8.899 \cdot 10^{-4}$	$1.831 \cdot 10^{-5}$	$1.5021 \cdot 10^{-5}$
σ [N m^{-1}]	0.072	-	-

Finally, boundary conditions need to be specified. On the column walls, a no-slip condition for the liquid phase and a free-slip condition for the gas phase hold are applied, assuming that direct contacts between the bubbles and the walls are negligible. To avoid the need to resolve the viscous sublayer, a single phase turbulent wall function, assuming a smooth wall, has been applied. At the top of the domain, which corresponds to the liquid level without gas

present, a degassing condition is applied. The four needles through which the gas is supplied are described by point sources.

4 SIMULATION RESULTS COMPARED TO MEASUREMENTS

All calculations have been performed with a customized version of ANSYS-CFX 14.5 (ANSYS, 2012). The simulations have been run in transient mode on the full 3D domain. Results have been averaged over a sufficiently long time that the resulting average does not change significantly anymore. Calculations were made on successively refined grids to ensure adequate resolution.

For comparison with the experiments, some post-processing of the simulation results is necessary. Denoting the time-average as $\langle\rangle$, simulation results for the gas fraction require an additional spatial average over the depth of field of the camera system as noted in section 2.2, i.e. $\alpha_G = \int \langle \alpha_G(t) \rangle \, d\xi$ with a suitable chosen integration range that depends on the direction of observation (front or side view). Results for the mean liquid velocity $\mathbf{u}_L = \langle \mathbf{u}_L(t) \rangle$ can be used directly. For the covariance tensor of liquid velocity fluctuations $\mathbf{u}'_L\mathbf{u}'_L$ one has to consider that in URANS mode there are two contributions, resolved and unresolved ones (Ziegenhein et al. 2015). The unresolved contribution is obtained from the averaged modeled turbulent kinetic energy $k_L = \langle k_L(t) \rangle$ and is isotropic, while the resolved contribution is calculated from the time-dependent liquid velocity field and is anisotropic. The resulting expression is

$$\mathbf{u}_L'\mathbf{u}_L' = \left\langle \left(\mathbf{u}_L(t) - \mathbf{u}_L\right)\left(\mathbf{u}_L(t) - \mathbf{u}_L\right) \right\rangle + \frac{2}{3} k_L \, \mathbf{1} \quad . \tag{18}$$

Experimental data are available for the square root of the diagonal yy- and xx-components of this tensor, i.e. $\sqrt{(v'_L v'_L)}$ and $\sqrt{(u'_L u'_L)}$.

A subset of test cases has been selected for the comparison from the larger experimental database. Conditions for the selected test cases are summarized in Table 3.

Table 3: Experimental parameters.

system	Q_G	$\langle d_B \rangle$	**available data**
	l/h	mm	
air / water	7.5	2.9	gas fraction, front and side view
air / water	10	3.1	gas fraction, front and side view
CO_2 / water	6.4	2.7	gas fraction and velocity, front view only

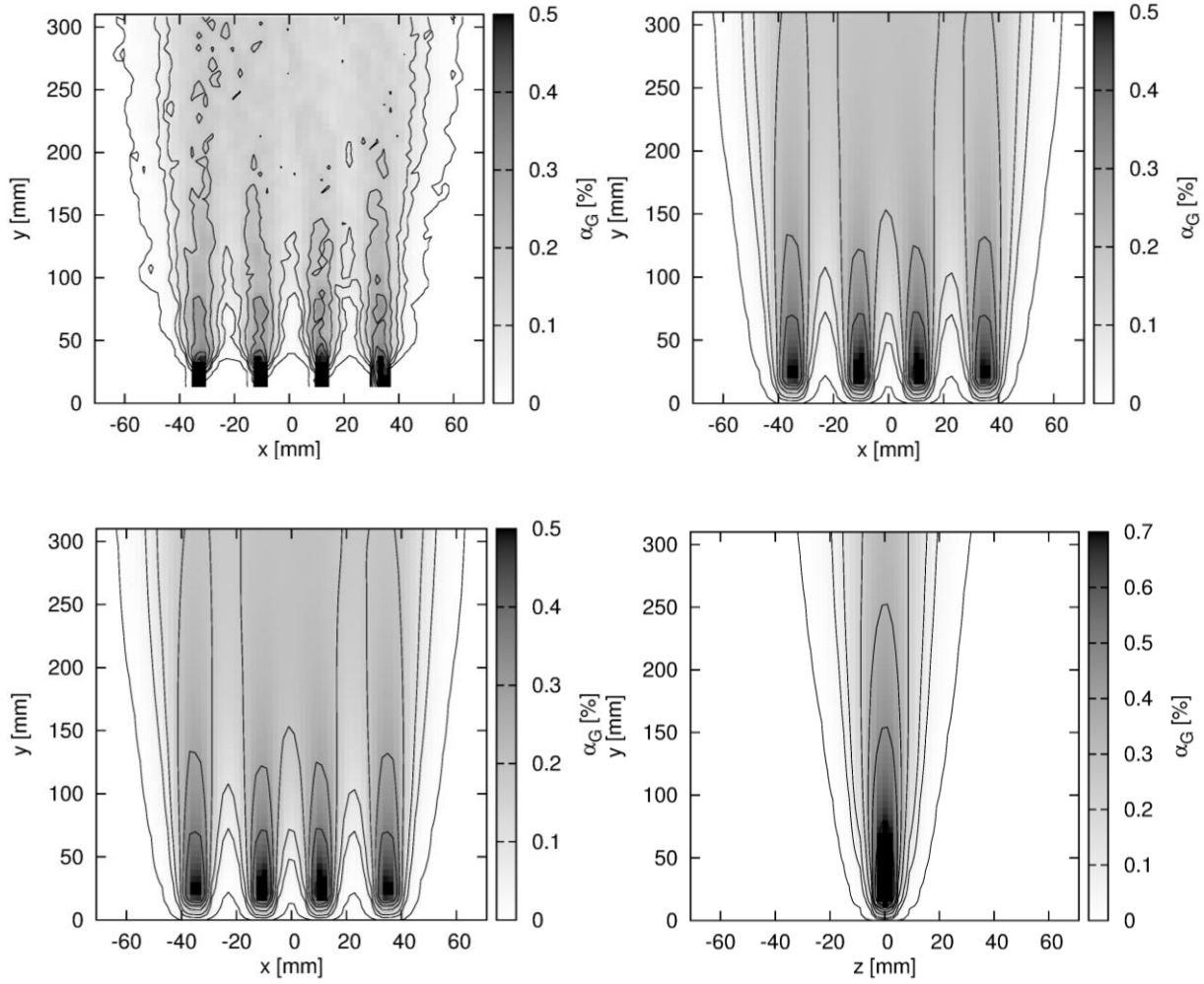

Figure 5: Comparison of gas fraction α_G calculated from the shadowgraphy measurements (top row) and from the simulation results (bottom row) for air bubbles in water at Q_G = 7.5 l/h. Left: 2D fields in front view; right: 2D fields in side view; top: experiment; bottom: simulation.

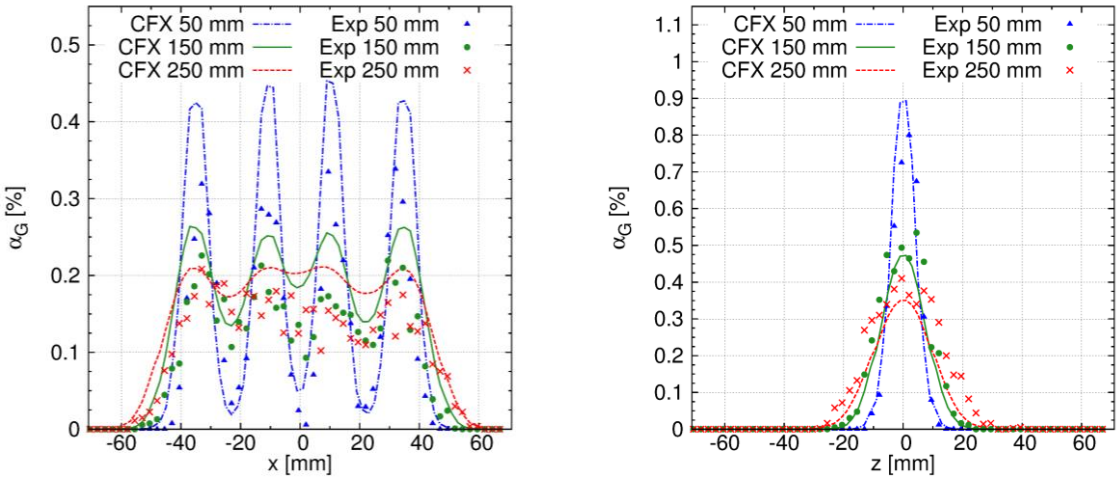

Figure 6: Comparison of gas fraction α_G calculated from the shadowgraphy measurements (symbols) and from the simulation results (lines) for air bubbles in water at Q_G = 7.5 l/h. Profiles taken at different heights as indicated in the legend; left: front view; right: side view.

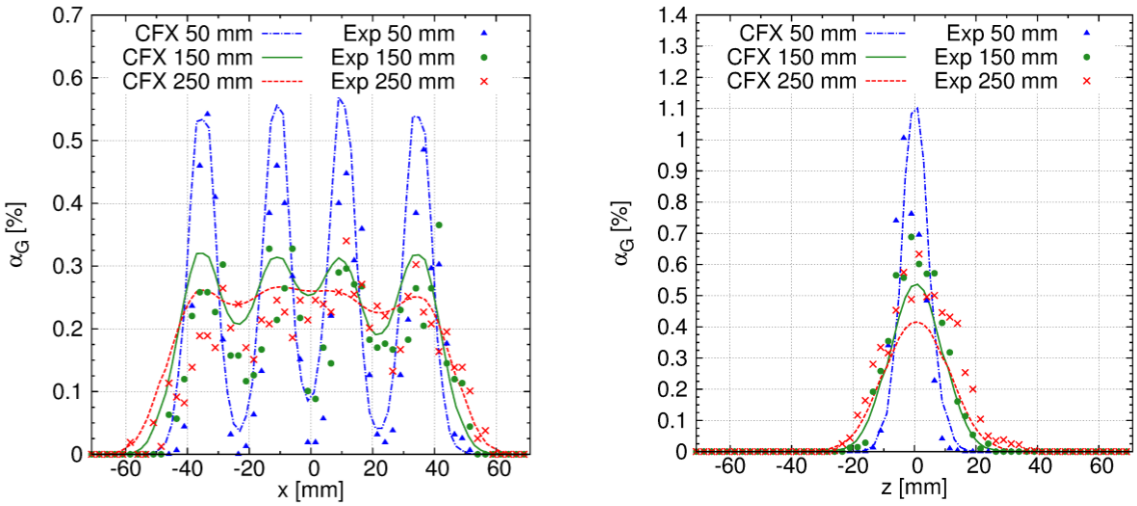

Figure 8: Comparison of gas fraction α_G calculated from the shadowgraphy measurements (symbols) and from the simulation results (lines) for air bubbles in water at Q_G = 10 l/h. Profiles taken at different heights as indicated in the legend; left: front view; right: side view.

Considering first the air / water system at a flow rate of Q_G = 7.5 l/h, Fig. 5 shows the two-dimensional distribution of gas fraction in the measurement plane for front view (left) and side view (right) up to a height of ~300 mm, where measurements have been taken. Bubble streams emanating from the nozzles are discernible in the lower part of the plots, while an almost homogeneous bubble sheet is observed in the upper part. Some residual fluctuation is still visible in the experimental data but the degree of symmetry with respect to the centerline is high. Comparison of experimental (top) and simulation (bottom) results, shows that the overall pattern of the gas distribution is reproduced quite well by the simulations. Note that the same greyscale has been used for experimental and simulation results.

A more quantitative assessment becomes possible by extracting horizontal profiles from the two-dimensional fields, which has been done in Fig. 6 for three different height levels, H = 50 mm, 150 mm, and 250 mm within the range covered by the measurements. It is seen that in front view (left), the amplitude of the peaks in the gas distribution in the simulations is somewhat too big at the lowest level, while it is somewhat too small at the highest level. The total amount of gas is a bit too high in the simulations at all levels. In side view (right) the simulations match the experimental data quite well.

A similar set of profiles is shown in Fig. 8 for the air / water system at a flow rate of Q_G = 10 l/h. Compared to the previous case, the gas fractions for this case are increased roughly in proportion to the flow rate, as expected in the homogeneous flow regime. The agreement between experiment and simulations is better than for the previous case for the front view. Only the somewhat too small amplitude of the gas-distribution peaks at the highest level remains. For the side view, the same good agreement is found as for the previous case.

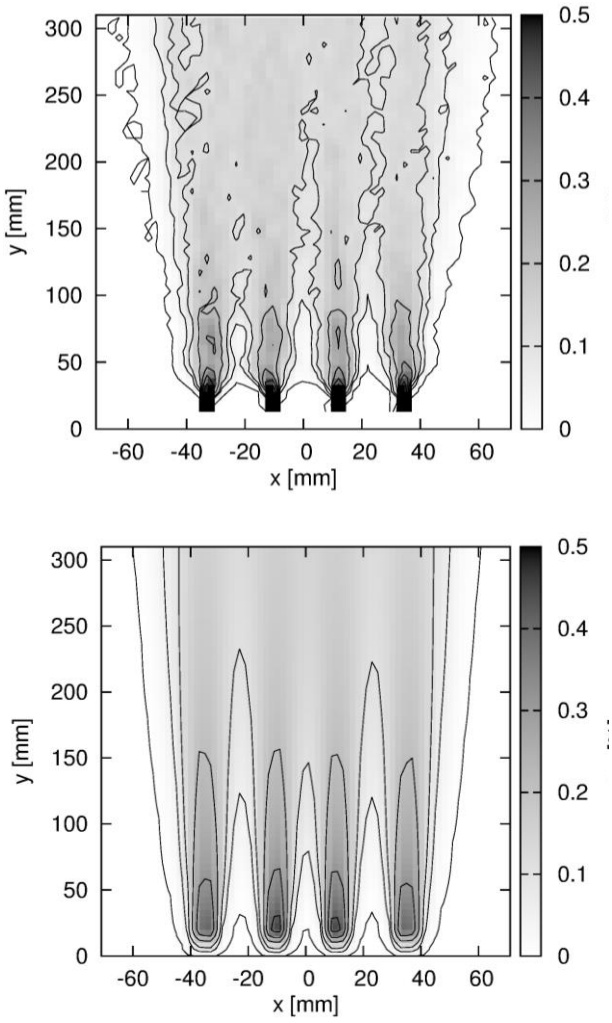

Figure 9: Comparison of gas fraction α_G calculated from the shadowgraphy measurements (top) and from the simulation results (bottom) for CO_2 bubbles in water at $Q_G \approx 6.4$ l/h. 2D fields in front view.

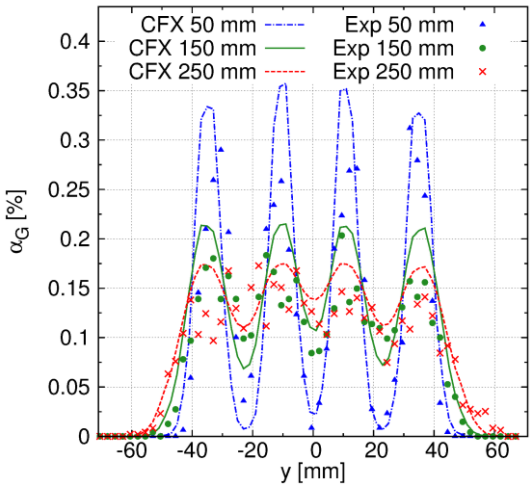

Figure 10: Comparison of gas fraction α_G calculated from the shadowgraphy measurements (symbols) and from the simulation results (lines) for CO_2 bubbles in water at $Q_G \approx 6.4$ l/h. Profiles in front view, taken at different heights as indicated in the legend.

Results for the gas fraction in the CO_2 / water system at a flow rate of Q_G = 6.4 l/h, are shown in Figs. 9 and 10. Only the front view is available for this case. The two-dimensional distributions shown in Fig. 9 reveal similar features as before. Comparison of experimental (top) and simulation (bottom) results, again shows that the overall pattern of the gas distribution is reproduced quite well by the simulations. Profiles extracted at the same height levels as previously are shown in Fig. 10. It is seen that for this case the quantitative agreement between experiment and simulation is quite good as well.

For the CO_2 / water system at Q_G = 6.4 l/h, also velocity data have been recorded. Vertical and horizontal components of the mean liquid velocity in the measurement plane up to the water level at 730 mm are shown in Fig. 11. Again only the front view is available. In the central part of the column, where most of the gas content resides, the liquid moves upwards. Near the column walls there is a region of liquid downflow. The mean horizontal motion of the liquid is notably different from zero only in a narrow zone near the free surface at the top.

A slight asymmetry is visible in both experimental and simulations results which comes from the finite averaging time and, in the experimental case, from slight manufacturing differences between the four nozzles. Comparing the qualitative mean liquid flow pattern in experiment and simulation there is good agreement in the extent of the up- and downflow regions as well as the sidewards motion near the top surface. However, even from the colorscale images it can be seen, that the magnitude of the vertical velocity is underpredicted by the simulations.

This may be analyzed in a quantitative manner by looking at the profiles of the vertical velocity component in Fig. 12. Here, the profiles have been taken at height levels H = 50 and 600 mm near the lower and upper end of the range covered by the measurements. At the lower level, it may be noted, that in the experiments the second to right nozzle apparently produced a faster liquid stream than the others. Since no difference is seen for this nozzle in the gas-fraction, the reason for this is unclear, but the effect may be taken as an estimate of the magnitude of factors which are hard to control in laboratory experiments and which will inevitably be present in technical applications. A slight reminiscence of the resulting peak in the liquid velocity persists up to the higher level. Comparing experimental and simulation results, it is seen that at the lower level, the simulations produce a too low liquid velocity in particular at the peaks in the profile. The difference to the experimental results is about the same as the variation between the outlier-nozzle and the others. At the higher level, the difference between simulation and experiment has become somewhat smaller and can partly be attributed to the remaining asymmetry in the latter.

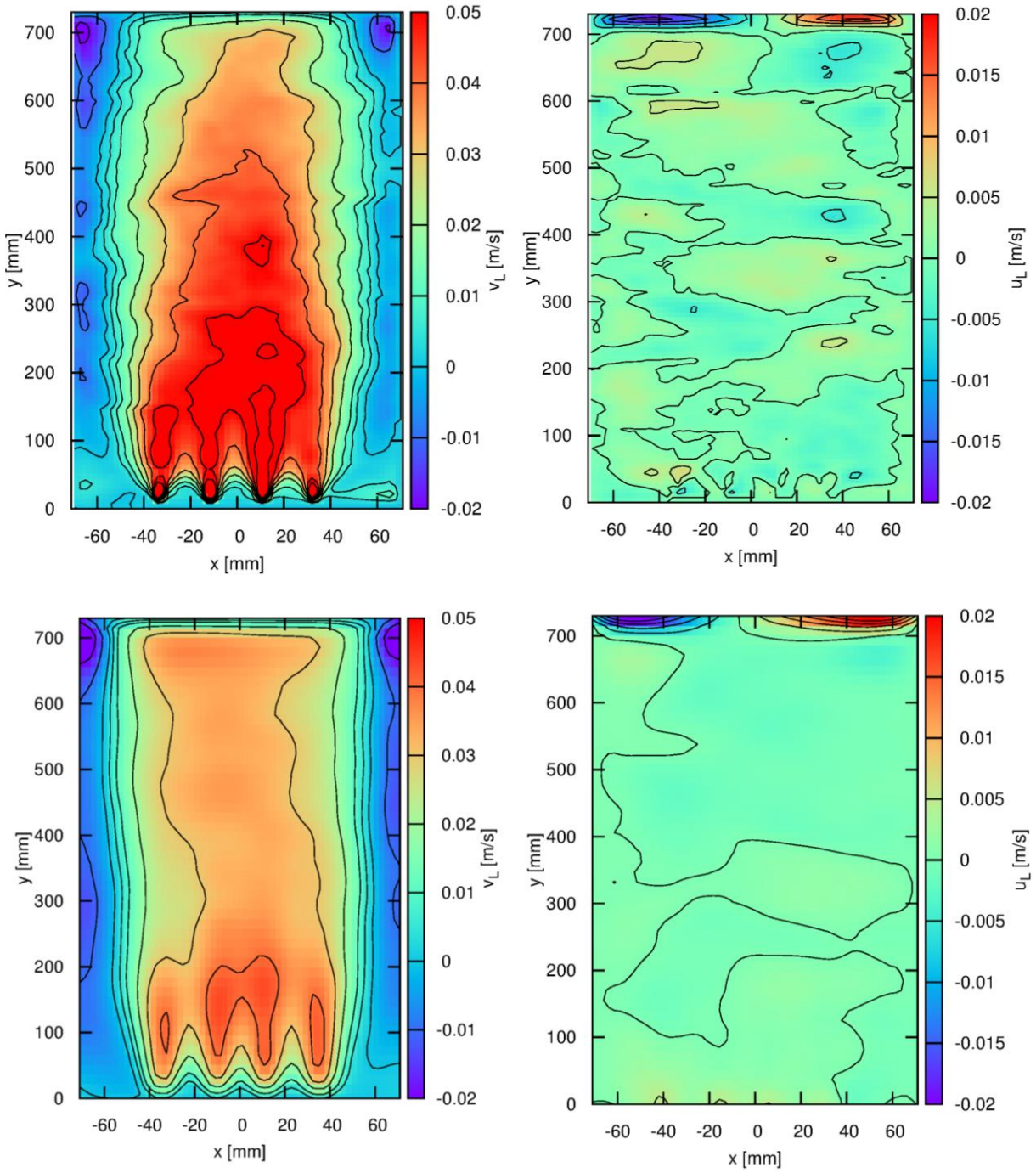

Figure 11: Comparison of average liquid velocity components v_L and u_L obtained from the PIV measurements and from the simulation results for CO_2 bubbles in water at $Q_G \approx 6.4$ l/h. Left: 2D fields with vertical component in front view; right: 2D fields with horizontal component; top: experiment; bottom: simulation.

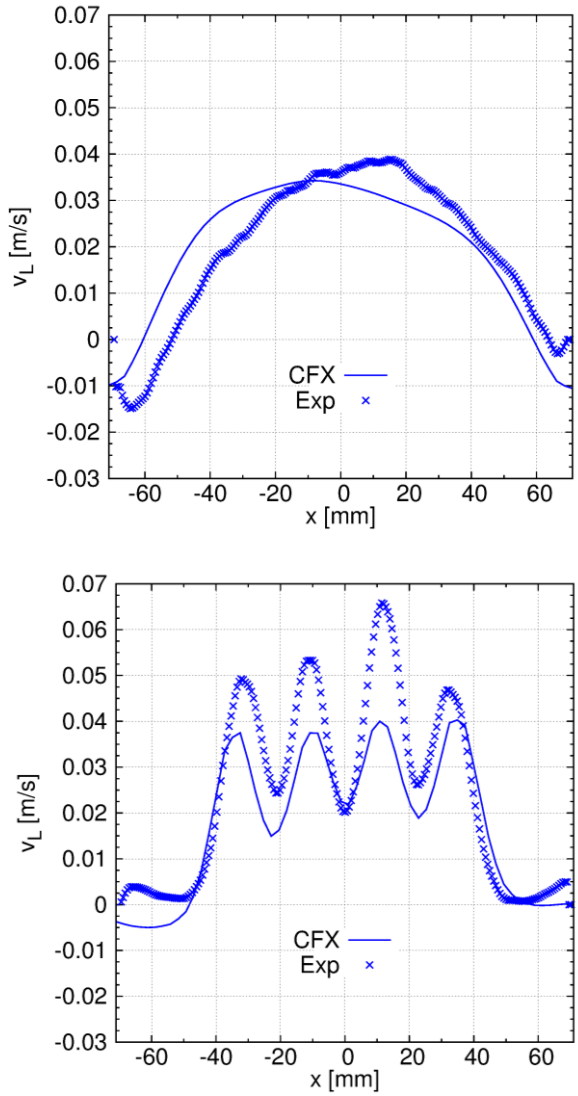

Figure 12: Comparison of average vertical liquid velocity component v_L obtained from the PIV measurements (symbols) and from the simulation results (lines) for CO_2 bubbles in water at $Q_G \approx 6.4$ l/h. Bottom: H = 50 mm; top: H = 600 mm.

Results on fluctuations of the liquid velocity in vertical and horizontal directions are displayed in Figs. 13 and 14. Fig. 13 shows the two-dimensional fields in the measurement plane. There is still notable scatter present in the experimental data and the expected symmetry with respect to the column center is not yet fully brought out. For the vertical fluctuations, the simulations are in good qualitative agreement with the measured data in the central part of the column. As for the horizontal fluctuations, the pattern is difficult to compare, but they are somewhat overpredicted in the simulations.
A quantitative comparison by means of profiles extracted at height levels H = 50 and 600 mm is shown in Fig. 14. For the simulation results the two contributions, resolved and unresolved, are shown separately in addition to the total fluctuations. For the vertical direction, agreement between simulation and experiment is good for both levels. In addition, it can be seen that near the inlet nozzles the unresolved contribution dominates over the resolved one, while at larger heights, both contributions are of similar magnitude. The horizontal fluctuations are somewhat overpredicted in the simulations. The resolved contribution thereby is only marginal.

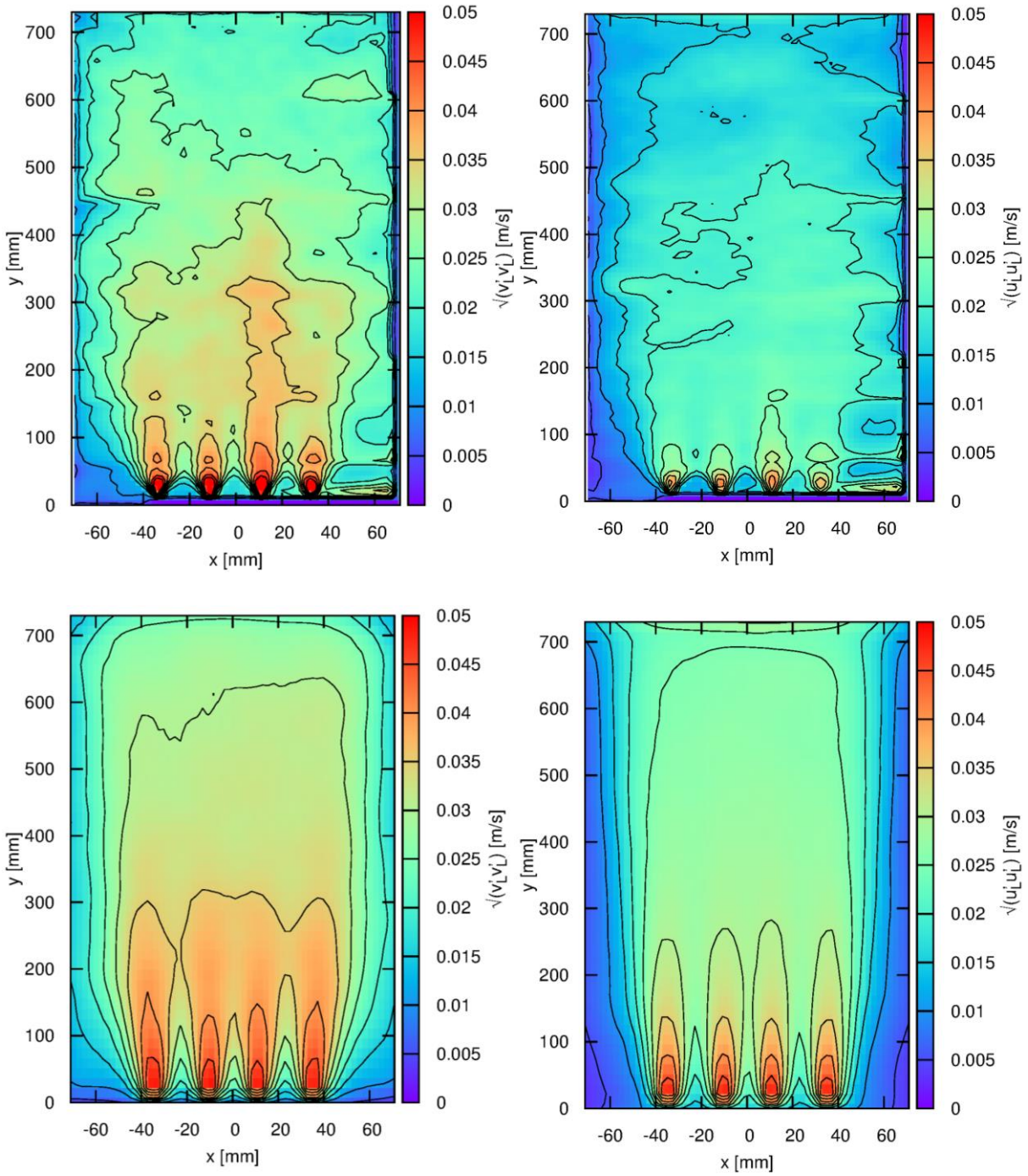

Figure 13: Comparison of liquid velocity fluctuations $\sqrt{(v'_L v'_L)}$ and $\sqrt{(u'_L u'_L)}$ obtained from the PIV measurements and from the simulation results for CO_2 bubbles in water at $Q_G \approx 6.4$ l/h. Left: 2D fields of vertical component in front view; right: 2D fields of horizontal component; top: experiment; bottom: simulation.

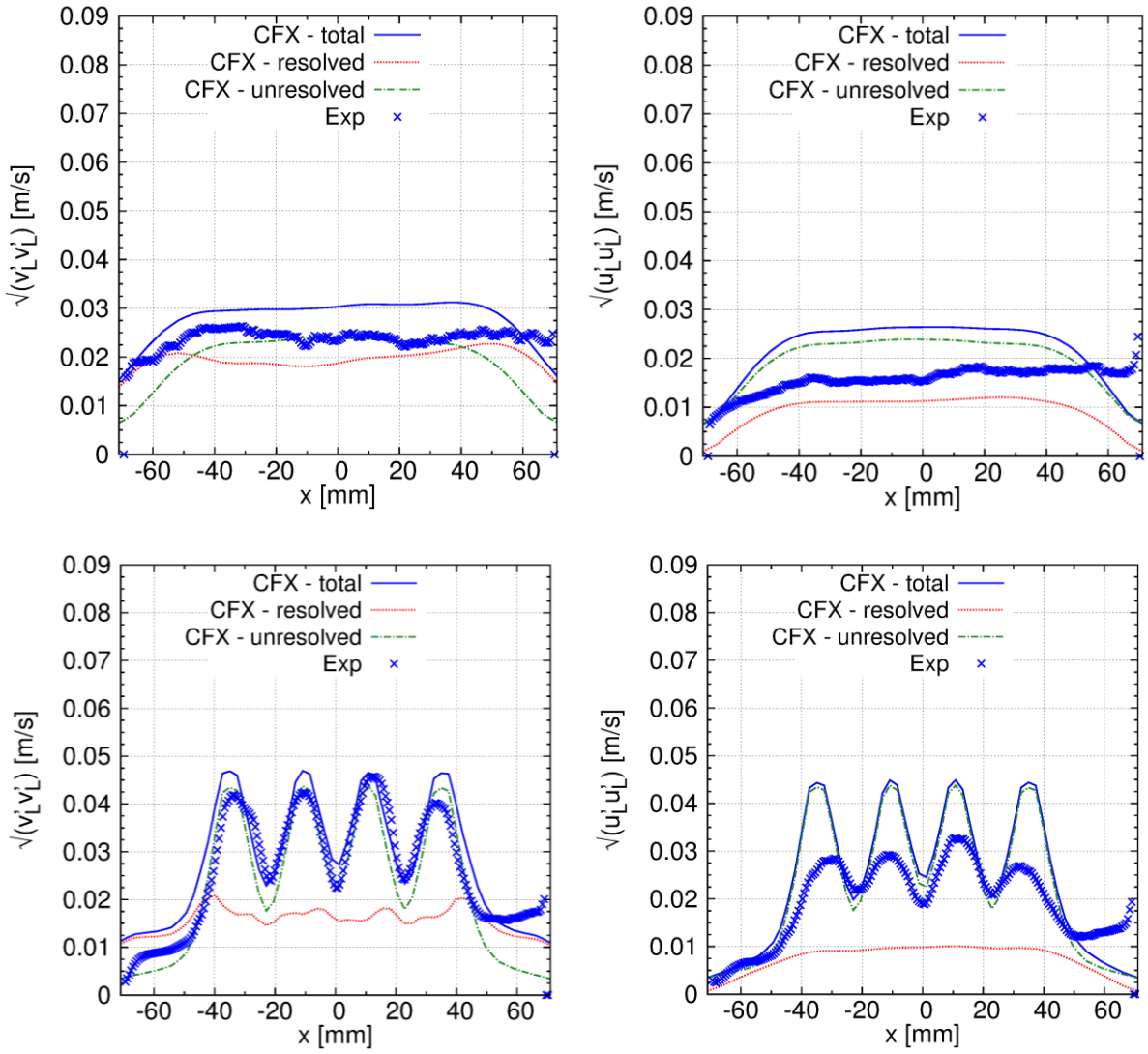

Figure 14: Comparison of liquid velocity fluctuations $\sqrt{(v'_L v'_L)}$ and $\sqrt{(u'_L u'_L)}$ obtained from the PIV measurements (symbols) and from the simulation results (lines) for CO_2 bubbles in water at $Q_G \approx 6.4$ l/h. Left: profiles of vertical component; right: profiles of horizontal component; bottom: H = 50 mm; top: H = 600 mm.

5 DISCUSSION AND CONCLUSIONS

A new set of measurement data has been presented for a laboratory scale bubble column which is suitable for the validation of multiphase CFD models. Arrangement of the nozzles, through which the gas is injected, in a single line produces a rather thin sheet of bubbles. This facilitates the application of laser light sheet techniques in addition to shadowgraphy. In this way, data are obtained that cover an entire plane within the column with high spatial resolution. High temporal resolution together with a long observation time gives averages with low residual noise and asymmetry. Furthermore also turbulent fluctuations can be determined in addition to the mean liquid velocity and gas fraction.

Corresponding simulations have been performed with an Euler-Euler model that was previously validated for both bubble columns and bubbly pipe flow. Comparison between experimental and simulation results for the two-dimensional fields, which show the spatial dependence of the observables in an entire plane, adds a new aspect to the previous model validation. In addition, one-dimensional profiles have been extracted for quantitative analysis. Three different test cases with varying gas flow rate and both air and CO_2 have been considered.
Overall the comparison is quite favourable for the gas fraction. Some deviations occur, but do not follow any clear trend.
For the mean liquid velocity in the vertical direction, the simulations give values which are systematically by ~20% too low, the deviation being somewhat more pronounced near the inlet nozzles than in the upper part of the column. At first sight, one might attribute this to a drag force which is too low. However, a higher drag force would also increase the residence time of the bubbles. The ensuing increase of the gas fraction then would worsen the agreement with the measurements of that quantity. Thus the origin of the discrepancy remains unclear at present. Mean liquid velocity in the horizontal direction is close to zero except two recirculation zones neat the free surface at the top of the water level. These are captured well by the simulations.
Concerning fluctuations of the liquid velocity, there is quite good agreement between simulation and experiment for the vertical direction. Fluctuations in the horizontal direction are overpredicted in the simulations by about 50%.
All in all the agreement between experiment and simulation is quite satisfactory for engineering predictions. Of course, the covered parameter range is limited in certain ways. One such aspect concerns the rather low gas-fraction present, another one the rather small and highly uniform size of the bubbles. In order to generalize the present model for higher gas fractions, swarm effects would have to be included in the various force coefficients, most importantly the drag coefficient (e.g. Roighair et al. 2011). To cover situations, where a wide distribution of bubble size is encountered, bubble coalescence and breakup processes ought to be considered (e.g. Liao et al. 2015). These developments will be pursued further in the future.

6 ACKNOWLEDGEMENT

This work has been carried out in the frame of the research projects RZ 11/1-1 and ZA-527/1-1 within the DFG Priority Programme 1740: “Reactive Bubbly Flows” funded by the german research foundation DFG.

7 NOMENCLATURE

Notation	Unit	Denomination
a_I	-	interfacial area density
C_D	-	drag coefficient
C_L	-	lift coefficient
C_{TD}	-	turbulent dispersion coefficient
C_{VM}	-	virtual mass force coefficient

C_W	-	wall force coefficient
C_μ	-	shear-induced turbulence coefficient (k-ε model)
d_B	m	bubble diameter
$d_\perp$	m	bubble diameter perpendicular to main motion
D	m	pipe / column diameter
Eo	-	Eötvös Number
F_D	N m^{-3}	drag force
F_L	N m^{-3}	lift force
F_{TD}	N m^{-3}	turbulent dispersion force
F_{VM}	N m^{-3}	virtual mass force
F_W	N m^{-3}	wall force
g	m s^{-2}	acceleration of gravity
G	kg s^{-1} m^{-2}	mass flux
H	m	height of test section
k	m^2 s^{-2}	turbulent kinetic energy
Mo	-	Morton Number
N_B	-	Number of bubbles
p	Pa	pressure
Q	l / h	volumetric flow rate
r	m	radial coordinate
Re	-	Reynolds number
s	m	hydrodynamic wall roughness
t	s	time
$\mathbf{u}$	m s^{-1}	phase velocity
u_τ	m s^{-1}	friction velocity
U	m s^{-1}	velocity scale
V_B	m^3	bubble volume
V_C	m3	volume of grid cell
x	m	axial coordinate
y	m	distance to the wall
α	-	phase fraction
δ	m	viscous length scale
ε	m^2 s^{-3}	turbulent dissipation rate
μ	kg m^{-1} s^{-1}	dynamic viscosity
ν	m^2 s^{-1}	kinematic viscosity
ρ	kg m^{-3}	density
σ	N m^{-1}	surface tension
τ_W	N m^{-2}	wall shear stress

8 REFERENCES

ANSYS, 2012. ANSYS CFX-Solver Theory Guide Release 14.5. *ANSYS Inc.*

Auton, T., Hunt, J., and Prud'Homme, M., 1988. The force exerted on a body in inviscid unsteady non-uniform rotational flow. *Journal of Fluid Mechanics* 197, 241–257.

Buffo, A. and Marchisio, D. L., 2014. Modeling and simulation of turbulent polydisperse gas-liquid systems via the generalized population balance equation. *Reviews in Chemical Engineering* 30, 73–126.

Burns, A.D., Frank, T., Hamill, I., and Shi, J.-M., 2004. The Favre averaged drag model for turbulence dispersion in Eulerian multi-phase flows. *Proc. 5th Int. Conf. on Multiphase Flow*, ICMF2004, Yokohama, Japan.

Chen, P., Sanyal, J. and Dudukovic, M., 2005. Numerical simulation of bubble columns flows: effect of different breakup and coalescence closures. *Chemical Engineering Science* 60, 1085–1101.

Colombo, M. and Fairweather, M., 2015. Multiphase turbulence in bubbly flows: RANS simulations. *International Journal of Multiphase Flow* 77, 222–243.

Deckwer, W.-D., 1992. Bubble Column Reactors. *Wiley*.

Deen, N., Solberg, T., and Hjertager, B. , 2001 Large eddy simulation of the Gas-Liquid flow in a square cross-sectioned bubble column. *Chemical Engineering Science* 56, 6341–6349.

Diaz, M., Montes, F. and Galan, M., 2009. Influence of the lift force closures on the numerical simulation of bubble plumes in a rectangular bubble column. *Chemical Engineering Science* 64, 930–944.

Drew, D. A., and Passman, S. L., 1998. Theory of Multicomponent Fluids, *Springer*.

Ekambara, K. and Dhotre, M., 2010. CFD simulation of bubble column. *Nuclear Engineering and Design* 240, 963–969.

Fox, R. O., 2007. Introduction and fundamentals of modeling approaches for polydisperse multiphase flows. In: Marchisio, D. L. and Fox, R. O. (Eds.) *Multiphase Reacting Flows: Modelling and Simulation*, Springer, 1–40.

Hibiki, T. and Ishii, M., 2007. Lift force in bubbly flow systems Chemical Engineering Science 62, 6457–6474.

Hosokawa, S., Tomiyama, A., Misaki, S., and Hamada, T., 2002. Lateral Migration of Single Bubbles Due to the Presence of Wall. *Proc. ASME Joint U.S.-European Fluids Engineering Division Conference*, FEDSM 2002, Montreal, Canada.

Ishii, M., and Hibiki, T., 2011 Thermo-fluid dynamics of two-phase flow. *Springer*, 2nd ed.

Ishii, M., and Zuber, N., 1979. Drag coefficient and relative velocity in bubbly, droplet or particulate flows. *AIChE Journal* 25, 843–855.

Jakobsen, H. A., Lindborg, H., and Dorao, C. A., 2005. Modeling of Bubble-Column Reactors: Progress and Limitations. *Industrial and Engineering Chemistry Research* 44, 5107–5151.

Kantarci, N., Borak, F., and Ulgen, K. O., 2005. Bubble column reactors. *Process Biochemistry* 40, 2263–2283.

Kataoka, I., Besnard, D. C. and Serizawa, A., 1992. Basic Equation of Turbulence and Modeling of Interfacial Transfer Terms in Gas-liquid Two-phase Flow. *Chemical Engineering Communications* 118, 221–236.

Kováts, P., Thévenin, D., and Zähringer, K., 2015. Fluid-dynamical Characterization of a Bubble Column for Investigation of Mass-transfer. *Conference on Modelling Fluid Flow* (CMFF'15), Budapest, Hungary.

Kováts, P., Thévenin, D., and Zähringer, K., 2016. Characterizing fluid dynamics in a bubble column to investigate mass transfer. *International Journal of Heat and Fluid Flow* submitted.

Laborde-Boutet, C., Larachi, F., Dromard, N., Delsart, O. and Schweich, D., 2009. CFD simulation of bubble column flows: investigations on turbulence models in RANS approach. *Chemical Engineering Science* 64, 4399–4413.

Liao, Y., Rzehak, R., Lucas, D. and Krepper, E. , 2015. Baseline Closure Model for Dispersed Bubbly Flow: Bubble-Coalescence and Breakup. *Chemical Engineering Science* 122, 336.

Liao, J., Ziegenhein, T., and Rzehak, R., 2016. Bubbly flow in an airlift column: a CFD study. *Journal of Chemical Technology & Biotechnology*, in press.

Lucas, D. and Tomiyama, A., 2011. On the role of the lateral lift force in poly-dispersed bubbly flows. *International Journal of Multiphase Flow* 37, 1178–1190.

Luo, H.-P. and Al-Dahhan, M. H., 2011. Verification and validation of CFD simulations for local flow dynamics in a draft tube airlift bioreactors. *Chemical Engineering Science* 66, 907–923.

Magnaudet, J., Rivero, M., and Fabre, J., 1995. Accelerated flows past a rigid sphere or a spherical bubble Part 1: Steady straining flow. *Journal of Fluid Mechanics* 284, 97–135.

Marschall, H., Mornhinweg, R., Kossmann, A., Oberhauser, S., Langbein, K., and Hinrichsen, O., 2010. Numerical Simulation of Dispersed Gas/Liquid Flows in Bubble-Columns at High Phase Fractions using OpenFOAM® Part 1 - Modeling Fundamentals. *Chemie Ingenieur Technik* 82, 2129–2140.

Masood, R. and Delgado, A., 2014. Numerical investigation of the interphase forces and turbulence closure in 3D square bubble columns. *Chemical Engineering Science* 108, 154–168.

Maxey, M. R., and Riley, J. J., 1983. Equation of motion for a small rigid sphere in a nonuniform flow. *Physics of Fluids* 26, 883–889.

Menter, F. R., 2009. Review of the shear-stress transport turbulence model experience from an industrial perspective. *International Journal of Computational Fluid Dynamics* 23,

305–316.

Morel, C., 1997. Turbulence modeling and first numerical simulations in turbulent two-phase flows. *Technical Report,* CEA / Grenoble, France.

Podowski, M., 2009. On the consistency of mechanistic multidimensional modeling of gas/liquid two-phase flows. *Nuclear Engineering and Design* 239, 933–940.

Politano, M., Carrica, P. and Converti, J., 2003. A model for turbulent polydisperse two-phase flow in vertical channels. *International Journal of Multiphase Flow* 29, 1153–1182.

Roghair, I., Lau, Y., Deen, N., Slagter, H., Baltussen, M., Van Sint Annaland, M., and Kuipers, J., 2011. On the drag force of bubbles in bubble swarms at intermediate and high Reynolds numbers. *Chemical Engineering Science* 66, 3204.

Rzehak, R., Krepper, E. and Lifante, C., 2012. Comparative study of wall-force models for the simulation of bubbly flows. *Nuclear Engineering and Design* 253, 41–49.

Rzehak, R. and Krepper, E., 2013a. Closure models for turbulent bubbly flows: a CFD study. *Nuclear Engineering and Design* 265, 701–711.

Rzehak, R., Krepper, E., 2013b. CFD modeling of bubble-induced turbulence. *International Journal of Multiphase Flow* 55, 138–155.

Rzehak, R., Krepper, E., Ziegenhein, T. and Lucas, D., 2014. A baseline model for monodisperse bubbly flows. *10th International Conference on CFD in Oil & Gas, Metallurgical and Process Industries* (CFD2014), Trondheim, Norway.

Rzehak, R. and Krepper, E., 2015. Bubbly flows with fixed polydispersity: validation of a baseline closure model. *Nuclear Engineering and Design* 287, 108–118.

Rzehak, R. and Kriebitzsch, S., 2015. Multiphase CFD-simulation of bubbly pipe flow: A code comparison. *International Journal of Multiphase Flow* 68, 135–152.

Rzehak, R., Krepper, E., Liao, Y., Ziegenhein, T., Kriebitzsch, S. and Lucas, D., 2015. Baseline model for the simulation of bubbly flows. *Chemical Engineering and Technology* 38, 1972–1978.

Rzehak, R., Ziegenhein, T., Kriebitzsch, S., Krepper, E., and Lucas, D., 2016. Unified modeling of bubbly flows in pipes, bubble columns, and airlift columns. *Chemical Engineeing Science*, submitted.

Sanyal, J., Marchisio, D. L., Fox, R. O. and Dhanasekharan, K., 2005. On the comparison between population balance models for CFD simulation of bubble columns. *Industrial and Engineering Chemistry Research* 44, 5063–5072.

Schmidtke, M., 2008. Investigation of the dynamics of fluid particles using the Volume of Fluid Method. PhD-thesis, *University Paderborn*, (in German).

Selma, B. Bannari, R. and Proulx, P., 2010a. A full integration of a dispersion and interface closures in the standard k-epsilon model of turbulence. *Chemical Engineering Science* 65, 5417–5428.

Selma, B., Bannari, R., and Proulx, P., 2010b. Simulation of bubbly flows: Comparison between direct quadrature method of moments (DQMOM) and method of classes (CM). *Chemical Engineering Science* 65, 1925–1941.

Serizawa, A. and Tomiyama, A., 2003. Some Remarks on Mechanisms of Phase Distribution in an Adiabatic Bubbly Pipe Flow. *Multiphase Science and Technology* 15, 79–98.

Shah, Y. T., Kelkar, B. G., Godbole, S. P., and Deckwer, W.-D., 1982. Design Parameters Estimations for Bubble-Column Reactors. *AlChE Journal* 28, 353–379.

Silva, M. K., d'Avila, M. A. and Mori, M., 2012. Study of the interfacial forces and turbulence models in a bubble column. *Computers and Chemical Engineering* 44, 34–44.

Sokolichin, A., Eigenberger, G., and Lapin, A., 2004. Simulation of Buoyancy Driven Bubbly Flow: Established Simplifications and Open Questions. *AIChE Journal* 50, 24–45.

Tabib, M. V., Roy, A. and Joshi, J., 2008. CFD simulation of bubble column - An analysis of interphase forces and turbulence models. *Chemical Engineering Journal* 139, 589–614.

Talvy, S., Cockx, A. and Line, A., 2007. Modeling Hydrodynamics of Gas-Liquid Airlift Reactor. *AIChE Journal* 53, 335–353.

Tomiyama, A., Sou, A., Zun, I., Kanami, N., and Sakaguchi, 1995. Effects of Eötvös number and dimensionless liquid volumetric flux on lateral motion of a bubble in a laminar duct flow. *Proc. 2nd Int. Conf. on Multiphase Flow*, Kyoto, Japan, 3.

Tomiyama, A., Kataoka, I., Zun, I., and Sakaguchi, T., 1998. Drag Coefficients of Single Bubbles under Normal and Micro Gravity Conditions. *JSME International Journal B* 41, 472–479.

Tomiyama, A., Tamai, H., Zun, I., and Hosokawa, S., 2002. Transverse migration of single bubbles in simple shear flows. *Chemical Engineering Science* 57, 1849–1858.

Troshko, A. A., and Hassan, Y. A., 2001. A two-equation turbulence model of turbulent bubbly flows. *International Journal of Multiphase Flow* 27, 1965–2000.

Wang, T., Wang, J., and Jin, Y., 2005. Population balance model for gas-liquid flows: influence of bubble coalescence and breakup models. *Industrial and Engineering Chemistry Research* 44, 7540–7549.

Wellek, R.M., Agrawal, A.K., and Skelland, A.H.P., 1966. Shapes of liquid drops moving in liquid media. *AIChE Journal* 12, 854–862.

Wilcox, D. C., 1998. Turbulence Modeling for CFD. *DCW-Industries*.

Yeoh, G. H., and Tu, J. Y., 2010. Computational Techniques for Multiphase Flows - Basics and Applications. *Butterworth-Heinemann, Elsevier Science and Technology*.

Zhang, D., Deen, N. and Kuipers, J. , 2006. Numerical simulation of the dynamic flow behavior in a bubble column: A study of closures for turbulence and interface forces. *Chemical Engineering Science* 61, 7593–7608.

Ziegenhein, T., Rzehak, R., and Lucas, D., 2015. Transient simulation for large scale flow in bubble columns. *Chemical Engineering Science* 122, 1–13.

Ziegenhein, T., Rzehak, R., Ma, T., and Lucas, D., 2016. A unified approach for modeling uniform and non-uniform bubbly flows. *Canadian Journal of Chemical Engineering*, submitted.

Zun, I. 1980. The transverse migration of bubbles influenced by walls in vertical bubbly flow. *International Journal of Multiphase Flow* 6, 583–588.